

# Neuromorphic Deployment of Spiking Neural Networks for Cognitive Load Classification in Air Traffic Control

Jiahui An<sup>\*†</sup>, Chonghao Cai<sup>\*</sup>, Olympia Gallou<sup>\*</sup>, Sara Irina Fabrikant<sup>‡</sup> Giacomo Indiveri<sup>\*</sup>, Elisa Donati<sup>\*</sup>

<sup>\*</sup>Institute of Neuroinformatics, University of Zurich and ETH Zurich, Zurich, Switzerland

<sup>†</sup>Digital Society Initiative, University of Zurich, Zurich, Switzerland

<sup>‡</sup> Department of Geography and Digital Society Initiative, University of Zürich, Zürich, Switzerland

**Abstract**—This paper presents a neuromorphic system for cognitive load classification in a real-world setting, an Air Traffic Control (ATC) task, using a hardware implementation of Spiking Neural Networks (SNNs). Electroencephalogram (EEG) and eye-tracking features, extracted from an open-source dataset, were used to train and evaluate both conventional machine learning models and SNNs. Among the SNN architectures explored, a minimalistic, single-layer model trained with a biologically inspired delta-rule learning algorithm achieved competitive performance (80.6%). To enable deployment on neuromorphic hardware, the model was quantized and implemented on the mixed-signal DYNAP-SE chip. Despite hardware constraints and analog variability, the chip-deployed SNN maintained a classification accuracy of up to 73.5% using spike-based input. These results demonstrate the feasibility of event-driven neuromorphic systems for ultra-low-power, embedded cognitive state monitoring in dynamic real-world scenarios.

**Index Terms**—Spiking Neural Networks, Neuromorphic Computing, Cognitive Load Monitoring, DYNAP-SE, Brain-Computer-Interface

## I. INTRODUCTION

Cognitive load refers to the mental effort required to process and respond to information [1]. Accurate and real-time assessment of cognitive load is critical in domains such as human-computer interaction, education, healthcare, and aviation [2–5]. For example, in high-stakes environments decision making contexts such as Air Traffic Control (ATC), where operators must maintain situational awareness and make rapid decisions under time pressure, inadequate cognitive load management can compromise task performance and increase the risk of errors. Therefore, reliable cognitive load monitoring is essential for developing adaptive systems that support human operators and enhance safety [6].

Conventional cognitive load inference methods rely on Machine Learning (ML) models trained on neurophysiological signals such as Electroencephalography (EEG) [3, 7–10]. However, their computational complexity often limits their deployment in embedded or wearable systems, where low latency and energy efficiency are critical.

We acknowledge the financial support of the Digital Society Initiative (DSI) at University of Zurich.

Neuromorphic computing, inspired by the architecture and dynamics of biological neural systems, offers a promising alternative. Spiking Neural Networks (SNNs), operating asynchronously and exploiting sparse spike-based communication, enable low-power, real-time processing [10, 11]. In this context, neuromorphic processors such as the Dynamic Neuromorphic Asynchronous Processor (DYNAP-SE) chip [12] provide an efficient hardware substrate for continuous cognitive state monitoring. The DYNAP-SE features four cores, each comprising 256 Adaptive Exponential Integrate-and-Fire (AdExp-IF) neurons with configurable excitatory and inhibitory synaptic dynamics, and uses an asynchronous Address-Event Representation (AER) communication protocol for scalable inter-core connectivity.

Previous work has demonstrated the utility of the DYNAP-SE chip in various biosignal processing tasks, including anomaly detection in Electrocardiography (ECG) signals [13, 14], classification of Photoplethysmography (PPG) waveforms [15], recognition of Electromyography (EMG) patterns [16–18], and biomarker extraction from EEG recordings in epilepsy patients [19, 20]. These studies highlight the potential of SNNs as biologically inspired alternatives to conventional ML approaches, including in domains such as cognitive load monitoring.

In this work, we present a neuromorphic system that classifies cognitive load during an ATC task, using multimodal physiological features extracted from an ecologically valid laboratory experiment involving both professional air traffic controllers and novices trained on the task [21]. We train and evaluate both conventional ML models and SNNs, with the latter implemented in software (snnTorch [22]) and deployed on the mixed-signal DYNAP-SE hardware platform.

Among the evaluated SNN architectures, a minimalistic no-hidden-layer model trained using a biologically inspired delta-rule learning algorithm achieved competitive performance (80.6%) and, after quantization, maintained robust classification accuracy (up to 73.5%) when deployed on hardware. Since the DYNAP-SE chip does not support online learning, the SNN was first trained offline in simulation and subsequently deployed onto the hardware with fixed weights for inference.

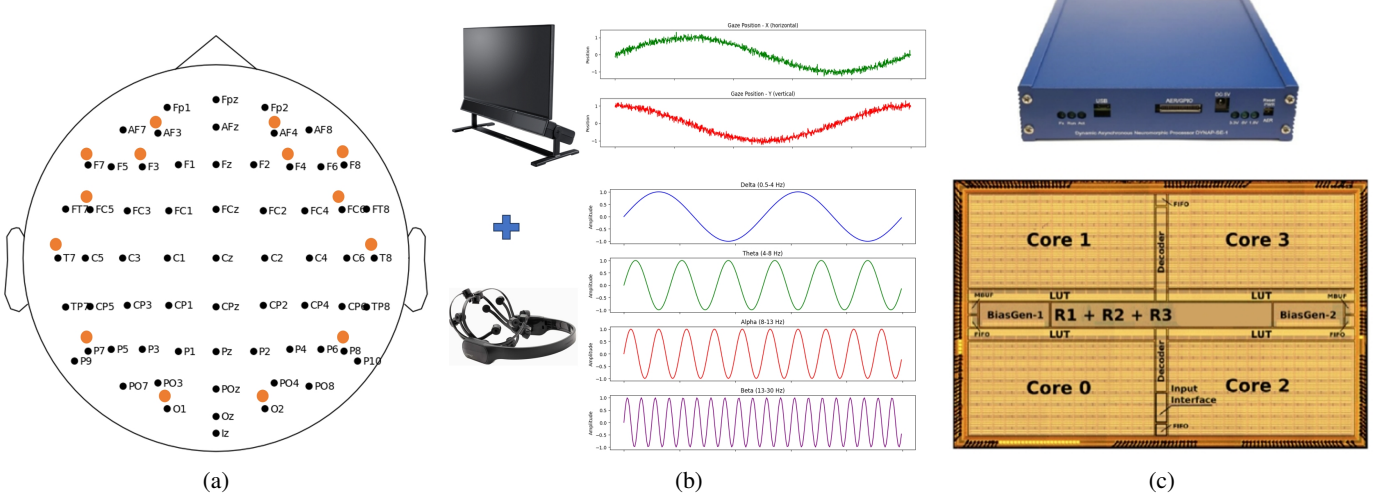


Fig. 1: System overview of the multimodal cognitive load classification setup. (a) The EEG electrode layout follows the standard 10–20 system, with Emotiv EEG sensor positions highlighted in orange. (b) EEG signals were recorded using Emotiv EPOC+ EEG headset, while gaze data were captured via a screen-based eye tracker. The panel also shows representative EEG and gaze-derived physiological features, including gaze position (X, Y), and oscillatory brain activity across standard frequency bands. (c) These features were used as input to a neuromorphic model. The extracted features were processed using the mixed-signal spiking neural network processor DYNAP-SE, which contains four neuromorphic cores, each supporting up to 256 analog neurons.

To the best of our knowledge, this work presents the first complete demonstration of real-time cognitive state classification from EEG and eye-tracking signals using quantized SNNs deployed on neuromorphic hardware. Figure 1 summarizes the multimodal data acquisition, feature extraction, and spike-based neuromorphic processing pipeline that enables energy-efficient cognitive load monitoring.

## II. MATERIALS & METHODS

We designed a complete neuromorphic cognitive load classification pipeline, encompassing dataset selection and pre-processing, feature extraction from multimodal physiological signals, model training with both conventional ML algorithms and SNNs, and hardware deployment on the mixed-signal DYNAP-SE platform. The following sections detail each stage of the methodology.

### A. Dataset and Experimental Paradigm

We used an open-access dataset from an ecologically validated ATC experiment [21], in which both professional air traffic controllers and novice participants monitored animated aircraft displays to detect potential collisions. EEG and eye-tracking data were simultaneously recorded during each 4-second trial under varying task difficulty (4 vs. 8 animated objects). EEG signals were collected using a 14-channel (AF3, F7, F3, FC5, T7, P7, O1, O2, P8, T8, FC6, F4, F8, AF4) Emotiv EPOC+ device[23] and gaze data were recorded with a Tobii TX300 eye tracker. The full dataset includes 592 trials from 39 participants. For this study, we retained 304 trials from 19 participants who had at least one valid modality (EEG or eye-tracking), including 9 professional air traffic controllers

and 10 control participants. A total of 217 trials containing both EEG and gaze-derived features were used for model training and hardware deployment. Preprocessing and feature extraction followed the protocol described in [21].

Five high-level features were extracted as model inputs:  $\alpha$  power, EEG engagement index, frontal alpha asymmetry (FAA), Gaze Transition Entropy (GTE), and Gaze Stationary Entropy (GSE). These features captured oscillatory neural dynamics and visual exploratory behavior. Specifically,  $\alpha$  power was computed as the mean spectral power in the 8–12 Hz band across selected channels; the EEG engagement index was defined as  $\beta/(\alpha + \theta)$ , reflecting attentional and arousal states; and FAA was calculated as the log ratio of right to left frontal  $\alpha$  power, indexing affective and cognitive regulation. Complementary features from eye-tracking included GTE, quantifying the randomness of gaze transitions between predefined Areas of Interests (AOIs), and GSE, measuring the spatial dispersion of fixations across AOIs.

Figure 1 summarizes the multimodal acquisition and processing pipeline. EEG and gaze signals were collected using wearable and screen-based devices, respectively, and processed to extract frequency-specific activities (delta, theta, alpha, beta, gamma), gaze positions (X, Y), and more high-level cognitive features. These features were then encoded into spike-based representations for classification using a neuromorphic model deployed on the DYNAP-SE board, a mixed-signal processor comprising four cores with 256 analog neurons each.

Task difficulty was operationalized as a binary classification label, defined by the number of aircraft displayed (4 = easy, 8 = hard), and encoded as 0 (low) and 1 (high) to maintain a balanced dataset.

## B. Model Training and Evaluation

We implemented and evaluated several classification models to distinguish between different levels of cognitive load based on five physiological features derived from EEG and eye-tracking signals. These features included alpha power, EEG engagement index, FAA, GTE, and GSE. All features were standardized with z-score normalization using the `StandardScaler` function from scikit-learn before being input into the models.

Model performance was assessed using four key metrics: accuracy, F1-score, precision, and recall. These metrics were computed on an independent 20% testing set. To account for variability across participants, all performance metrics were averaged across stratified  $k$ -fold cross-validation splits ( $k = 5$ ).

1) *Machine Learning models as Baselines*: As a baseline, we implemented standard models commonly used in the literature for cognitive load decoding. Establishing these baselines allows us to better characterize the dataset and provides a reference point to evaluate the performance of the proposed SNN models.

We first implemented a Logistic Regression (LR) model with L2 regularization. A grid search was conducted over the inverse regularization parameter  $C \in \{0.01, 0.1, 1, 10, 100\}$  using a 5-fold stratified cross-validation strategy to find the optimal configuration. In parallel, we trained Support Vector Machine (SVM) classifiers with three different kernels: linear, polynomial, and Radial basis function (RBF). For each kernel, a separate hyperparameter tuning process was employed. For the linear kernel, only the regularization strength  $C$  was tuned, whereas for the polynomial and RBF kernels, kernel-specific parameters (degree and gamma) and class weights were also optimized. All models were tuned using grid search with 5-fold stratified cross-validation.

2) *Training SNN with Delta Learning Rule*: To explore the potential of event-based models for cognitive load decoding, we tested different SNN architectures using the `snntorch` library [22], incorporating chip constraints to enable future deployment on neuromorphic hardware. The input to each SNN was a temporally encoded spike train generated from the five feature values using a rate-based Leaky Integrate-and-Fire (LIF) encoder. The LIF model follows the standard differential equation governing membrane voltage dynamics:

$$\tau \frac{dV(t)}{dt} = -(V(t) - V_{\text{rest}}) + X(t) \quad (1)$$

where  $V(t)$  is the membrane potential at time  $t$ ,  $V_{\text{rest}}$  is the resting potential (set to 0),  $\tau$  is the membrane time constant, and  $X(t)$  represents the input feature vector. A spike is emitted when  $V(t)$  exceeds the firing threshold  $V_{\text{th}} = -50$ , after which the potential is reset to  $V_{\text{reset}} = -65$ .

The temporal encoder was run for 16 simulation steps, corresponding to the number of trials per subject, with each trial representing 4 seconds of cognitive engagement. The encoded output was a spike count vector for each feature

across the 16 steps. These binary spike trains served as input to the SNN.

The network architecture comprised two fully connected layers: the first layer (fc1) projected the inputs to a hidden spiking layer via non-plastic, sparsely connected weights; the second layer (fc2) applied a delta learning rule based on the mismatch between predicted and target spike activity. The output spiking layer consisted of two LIF neurons with weak mutual inhibition to enable Winner-Take-All (WTA) dynamics. The inhibition matrix was predefined as:

$$\begin{bmatrix} 0 & -\gamma \\ -\gamma & 0 \end{bmatrix}$$

where  $\gamma \in [0.01, 0.05, 0.1]$  controlled the strength of mutual inhibition between competing output neurons.

The fc1 weights were initialized from a normal distribution with a tunable mean ( $fc1\_mean$ ) and a fixed standard deviation of  $0.2 \times fc1\_mean$ . A binary connection mask was applied according to a tunable connection probability parameter  $P_{\text{conn}}$ , enabling the modeling of biologically plausible sparse connectivity. All fc1 weights remained frozen during training, while fc2 weights were updated using the delta rule. The output LIF neurons also had learnable  $\beta$  parameters to adapt their membrane decay dynamics, tuned via grid search.

The output activity  $\hat{y} \in \mathbb{R}^2$  was computed as the LIF-encoded spike response after applying inhibition. Classification was performed by selecting the neuron with the highest firing rate. The delta rule weight update was defined as:

$$\Delta w = \eta \cdot (y_{\text{true}} - y_{\text{pred}}) \cdot x \quad (2)$$

where  $\eta$  is the learning rate and  $x$  is the presynaptic activation from fc1.

A grid search was performed to optimize biologically relevant hyperparameters, including the membrane time constant  $\tau \in \{15, 20, 25, 30, 35, 40\}$ , the  $fc1\_mean \in \{0.1, 0.3, 0.5, 0.7\}$ , the connection probability  $P_{\text{conn}} \in \{0.2, 0.5, 0.8\}$ , and the inhibition strength  $\gamma \in \{0.01, 0.05, 0.1\}$ . Each configuration was trained for 20 epochs using a learning rate of 0.001 and a batch size of 1. All experiments were repeated across three random seeds ( $\{0, 21, 42\}$ ) to ensure robustness.

a) *SNN with Hidden Layer*: To evaluate the impact of network depth on classification performance, we implemented SNN architectures by introducing a hidden spiking layer. Adding a hidden layer increases the model's capacity to capture nonlinear feature interactions, enabling the system to learn more complex decision boundaries while maintaining sparse and biologically plausible connectivity. Specifically, we varied the hidden layer size as a multiple of the input dimension (5), testing three scales:  $3\times$ ,  $5\times$ , and  $10\times$ .

A visual overview of this biologically grounded architecture is shown in Fig. 2(a).

b) *SNN without Hidden Layer*: Based on the ML results, we also implemented a single-layer SNN to evaluate the performance of a minimal architecture with primarily linear separation capabilities, as shown in Fig. 2(b). In this

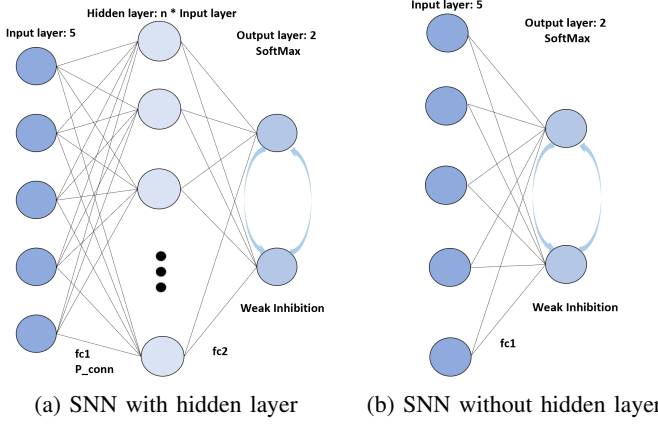


Fig. 2: Architectures of the SNNs used for cognitive load classification. (a) SNN with hidden layer: Input features are spike-encoded using LIF neurons and passed through a sparse ( $P_{conn}$ ) fixed-weight layer ( $fc1$ ), followed by a trainable output layer ( $fc2$ ). (b) SNN without hidden layer: Spike-encoded inputs are directly connected to the output layer ( $fc1$ ), with no intermediate hidden neurons. In both models, the output layer consists of two LIF neurons with weak mutual inhibition and a softmax readout, enabling WTA behavior. All output weights are trained using a delta learning rule adapted to spiking activity.

version, the spike-encoded inputs are directly connected to two output neurons modeled as LIF neurons, enabling spike-based representation and computation without intermediate hidden processing.

The input features were first encoded using the same spike encoding strategy described previously. The spiking classifier consisted of a single fully connected linear layer with two output neurons, followed by a LIF layer with a learnable decay factor  $\beta$  and a weak lateral inhibition term between the two outputs, as in the previous SNN models. Training was performed using a delta rule adapted to spiking output, where the weights of the input-to-output connections were iteratively updated based on the difference between the target label and the softmax-transformed spike output.

An extensive grid search was conducted to identify the best-performing model configuration, optimizing the membrane time constant  $\tau \in \{15, 18, 20, 23, 25, 28, 30, 31, 32, 33, 35\}$ , the learning rate  $\eta \in \{0.0001, 0.001, 0.01\}$ , the number of training epochs  $\in \{20, 25, 30\}$ , and the inhibition strength  $\gamma \in \{0.01, 0.05, 0.1\}$ . Each experiment was repeated across 12 random seeds to ensure robustness, and stratified 5-fold cross-validation was used to assess generalization performance.

### C. Deployment of Quantized SNN on DYNAP-SE chip

To evaluate real-world applicability, we deployed the optimal single-layer SNN on the neuromorphic chip DYNAP-SE. Since the DYNAP-SE chip does not support online learning, the network was first trained offline and subsequently deployed with fixed weights for inference. The deployment involved a

multi-step process comprising spike encoding, weight quantization, network mapping, and population-based spike decoding. The model selected for deployment corresponded to the best-performing fold identified during 5-fold cross-validation of the software simulation, achieving the highest performance among all folds.

*a) Spike Conversion and Encoding:* First, the continuous input features were encoded into spike trains using the same LIF dynamics described earlier (with grid-searched optimal  $\tau$  and 16 simulation steps). Each trial sample produced a spike raster with up to five input units corresponding to the multimodal features. To prepare the input for DYNAP-SE-compatible spike generators, we converted the spike rasters into timestamped firing events (in milliseconds). For each trial, binary spike matrices were generated, where a value of 1 indicated the occurrence of a spike for a particular feature at a given time step. These matrices were then transformed into event-based spike dictionaries containing spike times and corresponding unit indices.

To meet DYNAP-SE input constraints, a linear time scaling and offset shift were applied to each spike's time step. Specifically, the spike time  $t$  was calculated as:

$$t = (\text{time step} + 1) \times 0.01 \text{ seconds.}$$

Only trials with complete spike activity across all time steps were retained to ensure consistency across the dataset.

*b) Quantization of Network Weights:* To meet the DYNAP-SE chip's precision constraints (supporting only 3- or 4-bit signed weights), we applied 3-bit (int3) quantization to the learned float weights and biases from the best-performing fold. Quantization was performed by linearly scaling the float weights to the range  $[-3, 3]$ , rounding to the nearest integer, and clipping any values exceeding the representable bounds.

The resulting quantized parameters were loaded into a new SNN model with fixed weights and retrained using the same delta rule to assess the impact of quantization. The spike-based input encoding and LIF neuron dynamics were preserved to ensure compatibility with the event-driven architecture of the DYNAP-SE chip.

*c) Hardware Network Mapping:* The network deployed on the DYNAP-SE chip included five input spike generators (representing the five physiological features) and two output populations, each consisting of 20 neurons mapped to separate cores (Core 1 and Core 2). Spike generators were used to inject timestamped input events into the chip, while each output population acted as a readout unit corresponding to one of the two cognitive load classes.

Each feature-to-output population connection was weighted using an integer-valued  $5 \times 2$  weight matrix with values ranging from  $-3$  to  $+3$ . To implement these weights in hardware:

- Positive weights were realized through multiple parallel synaptic connections of type AMPA (fast excitatory).
- Negative weights were realized through multiple parallel synaptic connections of type GABA-A (fast inhibitory).

- The number of parallel synapses matched the absolute value of the weight; for example, a weight of +3 created three AMPA synapses.

The network was assembled using the DYNAP-SE API. Neurons in each output population received input from spike generators according to the quantized weight matrix and were further interconnected through GABA-B slow inhibitory synapses, implementing lateral inhibition between the two output populations to enable competitive decision dynamics.

*d) Monitoring and Evaluation:* Each encoded trial was presented to the chip via the FPGA-based spike generator interface. For each trial, the simulation ran for 0.16 seconds, during which output spikes were recorded from the two output populations. To ensure system stability, a buffer period of 0.5 seconds was added before and after stimulation to allow neuron dynamics to relax.

The recorded spike activity was post-processed by binning the spikes into discrete time windows:

- A window size of 2.5 ms (0.0025 s) was used.
- For each window, the average firing rate of each output population was computed by dividing the number of spikes by the product of the window length and the number of neurons (20 per population).

Classification was performed using a burst-based decoding strategy. Bursting events were identified by detecting windows with elevated firing rates, and the predicted class was assigned based on which output population exhibited stronger or more frequent bursts. In cases of ambiguity, a dynamic threshold adjustment was applied to resolve ties. Fallback rules ensured a decision even under low-activity conditions.

---

#### Algorithm 1 Burst-Based Classification

```

Input: Population firing rates; thresholds: zero, diff, offset, limit
Output: Predicted class iclass
Compute max_rate_pop1 and max_rate_pop2
if both max rates > zero then
    if rate difference  $\geq$  diff then
        iclass  $\leftarrow$  population with higher max rate
    else
        Count windows where rate  $\geq$  (max rate  $-$  offset)
        while counts equal and offset  $<$  limit do
            Increase offset; re-count
        end while
        iclass  $\leftarrow$  population with more counts
    end if
else if only one max rate > zero then
    iclass  $\leftarrow$  that population
else
    iclass  $\leftarrow$  population with more total spikes
end if

```

---

To assess the robustness and stability of the deployed SNN on the DYNAP-SE chip, we conducted five independent inference trials using the same optimized configuration. Evaluation metrics, including accuracy, precision, recall, and F1-score, were computed separately for each trial to capture variability arising from analog hardware stochasticity and spike dynamics.

### III. RESULTS

#### A. Machine Learning Model Performance

We evaluated the classification performance of several conventional ML models, including LR and SVMs with linear, polynomial, and RBF kernels.

Across all classifiers, the integration of multimodal cognitive features from EEG and Eyetracker—led to consistent performance improvements. Among these, the best-performing model was the polynomial-kernel SVM, achieving an accuracy of 84.3% ( $\pm$  5.6%), F1-score of 84.2% ( $\pm$  5.6%), and precision of 84.8% ( $\pm$  5.9%). The RBF SVM followed closely with an accuracy of 83.4% ( $\pm$  6.9%), while LR also demonstrated strong generalization with 82.5% ( $\pm$  6.6%) accuracy and 82.3% ( $\pm$  6.7%) F1-score.

The detailed results for each classifier are presented in Table I.

TABLE I: Performance Comparison of ML Models

Model	Accuracy	F1	Precision	Recall
LR	82.5%	82.3%	82.8%	82.3%
SVM (Linear)	82.9%	82.6%	83.9%	82.6%
SVM (Poly)	84.3%	84.2%	84.8%	84.2%
SVM (RBF)	83.4%	83.2%	84.1%	83.3%

#### B. Spiking Neural Network Performance

We explored SNNs for cognitive load classification using spike-encoded physiological features. Continuous input values were encoded into spike trains using a LIF neuron model, configured with a resting potential  $V_{\text{rest}} = 0$ , reset potential  $V_{\text{reset}} = -65.0$ , and firing threshold  $V_{\text{th}} = -50.0$ , over a simulation window of 16 steps. The membrane time constant  $\tau$  was treated as a hyperparameter and optimized via grid search.

*a) SNN with Hidden Layers:* To test the effect of deeper biological models, we implemented biologically plausible SNN models using fixed weights for *fc1*, sampled from a Gaussian distribution with a given mean (*fc1\_mean*) and connection probability (*P\_conn*). Only *fc2* weights were trained using the delta learning rule. The membrane dynamics were governed by the standard LIF differential equation, and hyperparameters were optimized using a nested grid search. The grid search tuned  $\tau$ , *fc1\_mean*, *P\_conn*, inhibition strength  $\gamma$ , and random seeds across various hidden layer sizes set to  $3\times$ ,  $5\times$ , and  $10\times$  the input size. Each configuration was evaluated using 5-fold cross-validation.

The best  $3\times$  hidden SNN achieved an accuracy of  $65.4\% \pm 6.8\%$ , with a high precision (79.2%) but lower recall (51.3%), suggesting cautious prediction behavior. The  $5\times$  hidden configuration improved recall (90.4%) and F1-score (74.9%) at 67.3% accuracy. The  $10\times$  configuration yielded the best F1-score of 68.3%, balancing both precision (76.5%) and recall (53.0%).

The best-performing model ( $10\times$  hidden, seed = 16,  $\tau$  = 30, *fc1\_mean* = 0.4, *P\_conn* = 0.5, inhibition = 0.01) achieved  $79.2\% \pm 4.9\%$  accuracy and an F1-score of  $80.2\% \pm 3.2\%$ ,

surpassing the baseline LR model and approaching the performance of kernelized SVM models. These results demonstrate that biological constraints, such as sparse fixed input weights and lateral inhibition, can lead to strong classification performance when appropriately tuned.

*b) Single-layer SNN:* To explore minimal neuromorphic implementations, we additionally trained a single-layer SNN. This architecture employed LIF spike encoding and a biologically inspired delta-rule learning mechanism applied directly to the output layer. Key hyperparameters—including the membrane time constant ( $\tau$ ), learning rate ( $\eta$ ), inhibition strength, and number of training epochs—were tuned through grid search across multiple random seeds.

The best configuration (seed = 31,  $\tau$  = 31, inhibition = 0.01,  $\eta$  = 0.01, 25 epochs) achieved an accuracy of  $80.6\% \pm 4.9\%$ , precision of  $85.2\% \pm 5.1\%$ , recall of  $77.4\% \pm 8.1\%$ , and F1-score of  $80.6\% \pm 1.6\%$ . Despite its simplicity, this architecture performed competitively, highlighting its potential for efficient, hardware-constrained deployment.

Table II compares the performance of this minimal SNN with its multi-layer counterparts, trained with varying hidden layer sizes ( $3\times$ ,  $5\times$ , and  $10\times$  the input dimension).

TABLE II: Performance Comparison of SNNs with and without Hidden Layer

Model	Accuracy	F1 Score	Precision	Recall
No Hidden	80.6%	80.6%	85.2%	77.4%
$3\times$ Hidden	65.3%	60.0%	79.2%	51.3%
$5\times$ Hidden	67.3%	74.9%	64.8%	90.4%
$10\times$ Hidden	72.9%	68.3%	85.6%	57.4%

### C. Quantized SNN Deployment Results

We evaluated the quantized SNN using stratified 5-fold cross-validation. To meet the precision constraints of the DYNAP-SE chip, int3 quantization was applied to the float weights learned from the best-performing fold. The resulting weight matrix was:

$$\text{Weights}_{\text{int3}} = \begin{bmatrix} 0 & -1 & -1 & 3 & -2 \\ 0 & 1 & 1 & -3 & 2 \end{bmatrix}$$

These quantized parameters were loaded into a new SNN model with fixed weights and retrained using the same delta learning rule to assess the impact of quantization. Spike-based input encoding and LIF neuron dynamics were preserved to maintain event-driven compatibility.

Despite reduced weight precision, the quantized model maintained strong performance, achieving an average accuracy of 76.9%, precision of 70.8%, recall of 96.5%, and F1-score of 81.7%. Compared to the original floating-point model, the accuracy dropped by only 3.7 percentage points, while high recall indicated robust sensitivity to the target class.

The quantized SNN was subsequently deployed on the DYNAP-SE hardware and evaluated on 217 valid samples (47% easy, 53% hard labels). Classification was performed fully on-chip by feeding spike train inputs and monitoring the

differential response of output neuron populations mapped to separate chip cores. To assess robustness under hardware variability, five independent inference trials were conducted using the same configuration. Across trials, the model achieved an average accuracy of  $73.5\% \pm 0.6\%$ , precision of  $70.4\% \pm 0.3\%$ , recall of  $86.1\% \pm 1.4\%$ , and F1-score of  $77.5\% \pm 0.6\%$ .

Figure 3 shows a representative trial output, illustrating the differential spiking activity and firing rate dynamics that led to a correct Class 1 prediction.

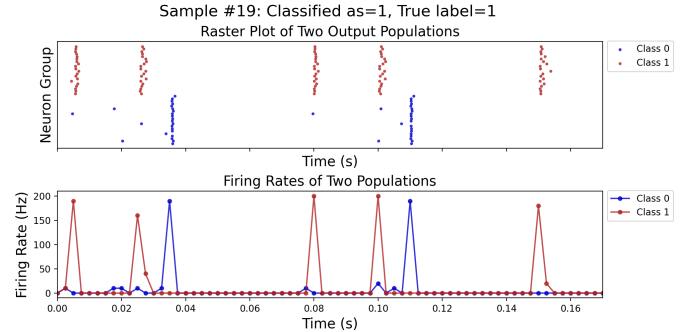


Fig. 3: Example Dynapse trial result illustrating the spike-based classification process. The raster plot (top) shows spike events from output neurons of Class 0 (blue) and Class 1 (red). The bottom panel shows sliding-window firing rates computed over 2.5 ms intervals. In this trial, stronger activity from the Class 1 population led to a correct Class 1 classification.

These results demonstrate that, despite quantization and hardware constraints, the deployed SNN maintained strong classification performance without retraining, confirming the feasibility of ultra-low-power, wearable neuromorphic systems for continuous cognitive state monitoring. However, the observed variability across hardware trials highlights the intrinsic stochasticity of analog neuromorphic platforms such as DYNAP-SE. Even with fixed weights and identical spike inputs, variations in spike timing, neuron dynamics, or lateral inhibition interactions can significantly affect network behavior. Robust deployment thus requires careful tuning of both network architecture and runtime parameters to mitigate hardware-induced variability.

## IV. DISCUSSION

Overall, our findings demonstrate that a simple, single-layer SNN, trained using biologically plausible learning rules, can be effectively quantized and deployed on neuromorphic hardware with state-of-the-art classification performance.

### A. Effectiveness of Multimodal Cognitive Features

Across all models, multimodal features derived from EEG and eye-tracking data yielded robust classification performance. These results confirm that combining oscillatory neural activity and visual entropy metrics enhances cognitive load decoding, particularly in dynamic ATC tasks.

### B. Insights into Linearity and Model Complexity

All conventional ML models, including LR and SVM variants, achieved similar accuracy levels (82.5%–84.3%, Table I). This narrow performance gap suggests that the task is largely linearly separable in the selected feature space. Notably, the LR model, despite its simplicity, achieved 82.5% accuracy, indicating that model interpretability and low complexity can be achieved without compromising performance.

### C. Simplicity and Robustness of single-layer SNN

The single-layer SNN trained with delta-rule learning reached 80.6% accuracy and 85.2% precision (Table II). Its strong performance despite minimal architecture highlights the adequacy of the selected features and the potential of low-capacity spiking networks for embedded neuromorphic applications.

### D. Impact of Hidden Layer Size in SNN

Expanding the hidden layer size to  $3\times$ ,  $5\times$ , and  $10\times$  the input dimension did not consistently improve performance. The  $5\times$  hidden model achieved the highest F1-score (74.9%) and recall (90.4%), while the  $10\times$  model optimized accuracy (72.9%) and precision (85.6%). Overfitting tendencies were observed in wider models, while moderate-width networks provided a better balance between sensitivity and stability. Interestingly, the single-layer SNN outperformed the  $3\times$  and  $5\times$  hidden variants, reinforcing the strength of the feature set and the utility of shallow spike-based architectures for this task.

### E. Hardware Deployment and Variability in DYNAP-SE

The quantized single-layer SNN was successfully mapped to the DYNAP-SE chip and evaluated on 217 trials, achieving 73.5% accuracy with spike-based input and output. These results validate that biologically inspired learning and quantization pipelines can translate effectively into low-power hardware implementations for cognitive state monitoring.

The implementation of the model using the analog circuits on the DYNAP-SE was affected by the circuit device-mismatch, which induced variability in synaptic strength, membrane dynamics, and spike latencies. Despite this, the accuracy remained consistent across five trials ( $\pm 0.6\%$ ), indicating that appropriate network design and decoding strategies can mitigate hardware-induced fluctuations. Future work will investigate calibration methods and adaptive reconfiguration to enhance robustness over longer-term deployments.

## V. CONCLUSIONS

This study presents a neuromorphic pipeline for cognitive state classification using spike-encoded multimodal physiological signals. We demonstrate that both conventional ML models and SNNs achieve strong performance on a real-world ATC task. Notably, a minimal single-layer SNN achieved 80.6% accuracy in software simulation and retained 73.5% accuracy after quantization and deployment on the DYNAP-SE neuromorphic chip.

To our knowledge, this is the first demonstration of real-time cognitive load classification from EEG and eye-tracking features using quantized SNNs deployed on neuromorphic hardware. These findings validate the feasibility of minimal, biologically grounded models for embedded cognitive monitoring in dynamic real-world environments.

While conventional ML approaches remain competitive baselines, SNNs offer unique advantages in energy efficiency and event-driven operation, making them well-suited for mobile and wearable applications. Overall, this work highlights the potential of low-power, real-time neuromorphic systems for continuous mental state monitoring, with promising applications in aviation safety, workload tracking, and next-generation wearable neurotechnologies.

## VI. ACKNOWLEDGEMENTS

We acknowledge the financial support of the Digital Society Initiative (DSI) at University of Zurich.

## REFERENCES

- [1] John Sweller. “Cognitive Load Theory”. In: *The Psychology of Learning and Motivation: Cognition in Education*. Ed. by J.P. Mestre and B.H. Ross. Elsevier Academic Press, 2011, pp. 37–76.
- [2] F. Dehais et al. “A neuroergonomics approach to mental workload, engagement and human performance”. In: *Frontiers in neuroscience* 14 (2020), p. 268.
- [3] G. Di Flumeri et al. “EEG-based mental workload neurometric to evaluate the impact of different traffic and road conditions in real driving settings”. In: *Frontiers in human neuroscience* 12 (2018), p. 509.
- [4] T. Kosch et al. “A survey on measuring cognitive workload in human-computer interaction”. In: *ACM Computing Surveys* 55.13s (2023), pp. 1–39.
- [5] L. Longo et al. “Experienced mental workload, perception of usability, their interaction and impact on task performance”. In: *PLoS one* 13.8 (2018), e0199661.
- [6] Cho Yin Yiu, Kam KH Ng, Qinbiao Li, and Xin Yuan. “Gaze behaviours, situation awareness and cognitive workload of air traffic controllers in radar screen monitoring tasks with varying task complexity”. In: *International Journal of Occupational Safety and Ergonomics* (2025), pp. 1–12.
- [7] Miloš Pušica et al. “Mental workload classification and tasks detection in multitasking: Deep learning insights from EEG study”. In: *Brain Sciences* 14.2 (2024).
- [8] J. Hassan et al. “EEG workload estimation and classification: a systematic review”. In: *Journal of Neural Engineering* (2024).
- [9] Yi Ding et al. “Measurement and identification of mental workload during simulated computer tasks with multimodal methods and machine learning”. In: *Ergonomics* 63.7 (2020), pp. 896–908.
- [10] P. O’Connor et al. “Real-time classification and sensor fusion with a spiking deep belief network”. In: *Frontiers in neuroscience* 7 (2013), p. 178.

- [11] E. Chicca et al. “Neuromorphic electronic circuits for building autonomous cognitive systems”. In: *Proceedings of the IEEE* 102.9 (Sept. 2014). ISSN: 0018-9219.
- [12] S. et al Moradi. “A Scalable Multicore Architecture With Heterogeneous Memory Structures for Dynamic Neuromorphic Asynchronous Processors (DYNAPs)”. In: *IEEE Transactions on Biomedical Circuits and Systems* 12.1 (Feb. 2018), pp. 106–122.
- [13] F. et al. Bauer. In: *Biomedical Circuits and Systems, IEEE Transactions on* 13.6 (Dec. 2019), pp. 1575–1582.
- [14] Alessio Carpegna et al. “Neuromorphic Heart Rate Monitors: Neural State Machines for Monotonic Change Detection”. In: *2024 IEEE Biomedical Circuits and Systems Conference (BioCAS)*. IEEE, Oct. 2024.
- [15] Chiara De Luca, Mirco Tincani, Giacomo Indiveri, and Elisa Donati. “A neuromorphic multi-scale approach for real-time heart rate and state detection”. In: *npj Unconventional Computing* 2.1 (2025), p. 6.
- [16] E. et al. Donati. “Discrimination of EMG Signals Using a Neuromorphic Implementation of a Spiking Neural Network”. In: *Biomedical Circuits and Systems, IEEE Transactions on* 13.5 (2019), pp. 795–803.
- [17] Ma Yongqiang et al. “EMG-Based Gestures Classification Using a Mixed-Signal Neuromorphic Processing System”. In: *IEEE Journal on Emerging and Selected Topics in Circuits and Systems* 10.4 (2020).
- [18] Enea Ceolini et al. “Hand-gesture recognition based on EMG and event-based camera sensor fusion: a benchmark in neuromorphic computing.” In: *Frontiers in Neuroscience* 14 (2020).
- [19] M. et al. Sharifshazileh. “An electronic neuromorphic system for real-time detection of High Frequency Oscillations (HFOs) in intracranial EEG”. In: *Nature Communications* 12.1 (2021), pp. 1–14.
- [20] Olympia Gallou et al. “Online Epileptic Seizure Detection in Long-term iEEG Recordings Using Mixed-signal Neuromorphic Circuits”. In: *2024 IEEE Biomedical Circuits and Systems Conference (BioCAS)*. IEEE, Oct. 2024, pp. 1–5.
- [21] Lanini-Maggi et al. “Assessing how visual search entropy and engagement predict performance in a multiple-objects tracking air traffic control task”. In: *Computers in Human Behavior Reports* 4 (2021).
- [22] Jason K Eshraghian et al. “Training spiking neural networks using lessons from deep learning”. In: *Proceedings of the IEEE* 111.9 (2023), pp. 1016–1054.
- [23] Emotiv EPOC+. <https://www.emotiv.com/>. Accessed: 2021-01-21. 2021.